# Theoretical and Numerical Hydromechanics Analysis of Self-Pitching Propellers

**Luca Greco, Stefania Leone, Claudio Testa,
Francesco Salvatore, Salvatore Mauro**

Italian Ship Model Basin (CNR - INSEAN), Rome, Italy

## ABSTRACT

The development of design-oriented modelling techniques to predict Self-Pitching Propellers (SPP) hydrodynamic and dynamic behaviour is here addressed. Two hydrodynamics approaches are described and validated against literature data. Both Controllable-Pitch propellers (CPP) and SPP test cases are considered. In addition a general theoretical Reduced Order Model (ROM) for blade hydrodynamics unsteady loads is proposed to investigate blade equilibrium stability. Numerical results are shown in terms of performance, spindle moment and pitch setting equilibrium conditions.

### Keywords

Self-Pitching Propellers, hydrodynamics, blade dynamics, Reduced Order Models

## 1 INTRODUCTION

Self-Pitching Propellers blades are free to rotate 360° about the spindle axis. Actual blade pitch automatically adapts to vessel speed conditions through a balance between centrifugal forces due to blade inertial characteristics and hydrodynamic moment about the spindle axis. SPP can operate as propellers as well as energy generation devices thus are widely recognised as an attractive propulsive solution for small and medium size vessels and sailing boats.

Blade dynamics equation coupled with suitable hydrodynamics solvers is proposed to determine blade free-pitching conditions and, in turns, equilibrium stability margins. Specifically, fast computational hydrodynamics approaches, based on Blade Element Momentum Theory (BEMT) and Boundary Element Method (BEM), are herein proposed; in this context BEM approach is quite new, whereas BEMT has been applied by Miles et al (1992) in the past for the design of self-pitching propellers. With respect to Miles et al (1992), the BEMT approach used throughout the paper enhances prediction of induced velocity due to trailing wake affecting propeller performance. To overcome BEMT unconservative margins predictions related to three-dimensional unsteady wake shedding effects (see Gennaretti et al 2008), a Reduced Order Model (ROM) based on BEM solver for propeller hydrodynamics coupled to perturbative blade motion equation, is proposed from a theoretical standpoint.

## 2 BLADE DYNAMICS

In the present section, the equations describing a general rigid body motion are specialized to describe SPP behaviour and then the procedure for the identification of the equilibrium condition and the stability margins is described. In order to derive a mathematical description of
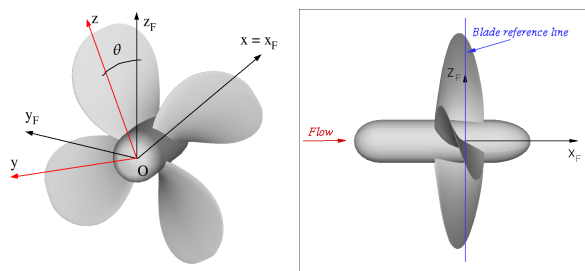


Figure 1: Depiction of frame of references.

blade kinematics, three different frames of reference are introduced (see figure 1): *i)* disk reference $O, x_F, y_F, z_F$ centered at the propeller disk plane and translating along $x$ axis with velocity $V_\infty$; *ii)* spindle reference $O, x, y, z$ rotating with blade angular velocity $\Omega$ about $x$ axis and traslating along $x$ axis with velocity $V_\infty$; *iii)* blade reference $O, x_b, y_b, z_b$, rigidly connected to the reference blade following its rotation about the spindle axis. The image of conservation of angular momentum equations into the blade frame of reference yields the following equation describing blade motion about the spindle axis:

$$J_{zz}\ddot{\epsilon} + J_{xy}\Omega^2 cos(2\epsilon) + (J_{xx} - J_{yy})\frac{\Omega^2}{2}\,sin(2\epsilon) =$$
$$= m_O^z = (m_H^z + m_W^z)_O \quad (1)$$

where $J_{zz}$, $J_{xx}$, $J_{yy}$ and $J_{xy}$ are the components of the inertia tensor, $\epsilon$ is the variation of angular pitch setting due to the rotation about the spindle axis and $\Omega$ is propeller angular velocity. The right hand side of Equation (1) represents the forcing term due to hydrodynamics and blade's weight moment about the spindle axis ($m_H^z$ and $m_W^z$, respectively). Note that, the spindle moment due to weight is time dependent because of change of position of blade center of gravity during propeller revolution.

Previous experimental and numerical research on SPP

(Miles et al 1992) shows that blade oscillations frequencies are rather less than once per rev; hence the static approximation may be reasonably adopted. Under this assumption, the static approximation of Equation (1) recasts

$$J_{xy}\Omega^2 cos(2\epsilon_e) + (J_{xx} - J_{yy})\frac{\Omega^2}{2} sin(2\epsilon_e) =$$
$$= m_H^z(\epsilon_e, \theta) \qquad (2)$$

where $\epsilon_e$ is the variation of blade pitch setting at the equilibrium condition and $\theta$ is the blade design angular pitch. For a given propeller (whose geometrical and inertial features are assumed to be known) working at a specified advance ratio $J$, the blade pitch equilibrium angle $\epsilon_e$ is obtained numerically by solving Equation (2) through an iterative procedure once the spindle moment $m_H^z$ due to hydroloads is known.

Once the equilibrium condition is determined for a given value of $J$, the stability analysis can be performed. To this aim, Equation (1) is linearized about $\epsilon_e$ to obtain the equation of motion describing the dynamics of blade rigid body perturbation motion about the spindle axis

$$J_{zz}\ddot{\epsilon} + \left[\Omega^2(J_{xx} - J_{yy})cos(2\epsilon_e) -\right.$$
$$\left. -2J_{xy}\Omega^2 sin(2\epsilon_e)\right]\epsilon = \tilde{m}_H^z(\epsilon, \epsilon_e, \theta) \qquad (3)$$

where $\tilde{m}_H^z$ is the spindle moment acting on the blade induced by its perturbative motion; a suitable theoretical description of it as an explicit function of blade pitch degree of freedom $\epsilon$ is presented in the following. It is worth noting that time–dependent linear terms due to blade's weight are negligible with respect to centrifugal terms. The presented approach yields a linear differential equation describing perturbative blade pitch motion. Stability analysis can be then performed through classical eigenvalue approaches.

### 3 HYDRODYNAMICS MODELS

#### 3.1 Blade Element Momentum Theory

BEMT model is a widely used approach for the analysis and design of SPP (see Miles et al 1992). This approach, combining the basic principles from both blade element (BET) and momentum theories, is inherently steady, two-dimensional, stems from the equivalence between the circulation and momentum theories of lift and allows to estimate the inflow distribution along the blade. It is well-known that such 2D approaches over-predict thrust and under-predict torque with respect to more complex and efficient hydrodynamics modelling, yielding a rough estimate of the hydrodynamic performance of a propeller. Despite these intrinsic limitations, the simplified BEMT approach may be yet used as an effective tool, during the pre-design process, as far as complexity and computational efforts are concerned; in fact, it provides a hydrodynamic *predictor* of thrust, torque and efficiency of marine propellers under a large range of operating conditions. In the following, some main aspects concerning BEMT hydrodynamics modelling used herein the paper are highlighted; details are found in Leishmann (2006).

On the basis of one-dimensional momentum theory (MT) (see Leishmann 2006) with the 2D assumption that successive rotor annuli have no mutual effects on each other, incremental thrust on a rotor annulus of the rotor disk and torque absorbed by the annulus may be written as

$$\frac{dT}{dr} = 4\pi\rho\, rV_A^2(1 + a)a$$
$$\frac{dQ}{dr} = 4\pi\rho\, r^3V_A(1 + a)a'\Omega \qquad (4)$$

where $\rho$ is the fluid density, $r$ is the local distance of the annulus from the rotatioanl axis, $V_A$ is the speed of advance, $\Omega$ is rotational speed of the propeller, $a = v_i/V_A$ is the axial-inflow factor, $v_i$ indicates the induced-velocity at the propeller blade and $a'$ is the rotational-inflow factor. From Equation (4), the efficiency $\eta = dT\, V_A/\Omega\, dQ$ of the annular element recasts

$$\eta = \frac{V_A^2}{\Omega^2 r^2}\frac{a}{a'} \qquad (5)$$

Accounting for a Z-bladed propeller, thrust and torque related to a blade element of length $dr$ in spanwise direction as given by the BET model are

$$\frac{dT}{dr} = \frac{1}{2}\rho c Z V_A^2(1 + a)^2 cl\frac{cos(\phi + \gamma)}{sin^2\phi\, cos\gamma}$$
$$\frac{dQ}{dr} = \frac{1}{2}\rho c Z r V_A^2(1 + a)^2 cl\frac{sin(\phi + \gamma)}{sin^2\phi\, cos\gamma} \qquad (6)$$

where $c$ is the local chord of the blade section at radius $r$, $cl$ is the local lift-coefficient, $\phi$ is the local inflow-angle whereas $tg\gamma = cd/cl$, being $cd$ the sectional drag coefficient. From the blade velocity diagram shown in Figure 2, the velocity of the fluid relative to the blade section may be written as $V_R = V_A(1 + a)/sin\phi$, the angle of incidence $\alpha$ is $(\theta - \phi)$ ($\theta$ represents the geometrical pitch angle) and $tg\beta = V_A/\Omega r$. Lift and drag coefficients may be found from tabular data (once the angle of attack (AOA) is known) for each blade section; alternatively, a polynomial approximation such as $cl \cong cl_\alpha(\alpha - \alpha_0)$ and $cd \cong c_1 + c_2\alpha + c_3\alpha^2$ may be reasonably used, where $\alpha_0$ is the zero lift angle shown in Figure 2, $cl_\alpha$ is the lift slope coefficient (a value between $5.7$ and $2\pi$ is used) and $c_i, (i = 1, 2, 3)$ are coefficients assumed to be known. Akin to the MT model, from Equation (6) the efficiency of the blade element recasts

$$\eta = \frac{1 - a'}{1 + a}\frac{tg\phi}{tg(\phi + \gamma)} \qquad (7)$$

For a given propeller working at an advance ratio $J = V_A/nD$ ($D$ indicates the propeller diameter and $n$ the rotation speed in terms of $rps$), the performance of each blade element can only be determined when values of the inflow factors $a$, $a'$, the section AOA $\alpha$ and $cl$, $cd$ are known; further, rotor performance can be obtained by integrating the sectional loads at each blade element over the length of the blade. At this stage it is useful to highlight that the removal of the 2-D restriction requires a considerably more
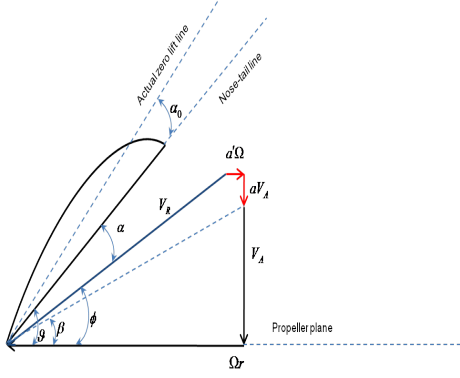
Figure 2: Flow vectors and angles.

thrust $dT$, torque $dQ$ and centrifugal force $dF_c$ determine the elemental moment contribution $dM_s$ about the pivot axis. It is here assumed that thrust and torque delivered by the section blade act at the centre of pressure of that section whilst the centrifugal force acts at the centre of gravity of each hydrofoil, (see Figure 3). Since the effect of the
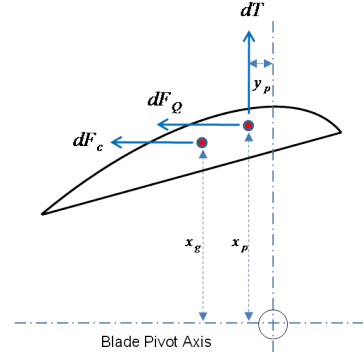


Figure 3: Forces acting on a blade section: contribution to the spindle moment.

advanced treatment of the problem using a vortex wake theory; however, the problem of the loss of lift near the tip, may be approximately predicted through the Goldstein factors (see Carlton 1994) $k_\beta$ and $k_\epsilon$ at the propeller disk and in the ultimate wake, respectively. Thus, the first equation of Equation (4) becomes

$$\frac{dT}{dr} = 4\pi\rho \, r V_A^2 (1 + a \, k_\beta) a \, k_\epsilon \qquad (8)$$

where the Goldstein correction factors may be obtained through tabular data as functions of blades number, boss radius, inflow angle and radial station.

Equations (5), the first of (6), (7) and (8) define a non-linear problem that might be solved iteratively for each blade strip. However, by equating Equations (5) and (7), using the relation (see Figure 2)

$$tg\phi = \frac{1+a}{1-a'} tg\beta \qquad (9)$$

and equating the sectional thrust from MT and BET theories, a non-linear equation in terms of the inflow angle $\phi$ is derived. Its numerical solution is given by the Newton-Raphson method. The choice of the starting point $\phi_0$ for the solution seeking may be a crucial point; a reasonably initial-guess is that coming from the linearized BEMT approach. Under this assumptions, one obtains the following relation in terms of nondimensional parameter $\lambda = (V_A + v_i)/\Omega R \cong \phi_0 r/R$ (see Leishmann 2006)

$$\lambda(r) = \sqrt{\left(\frac{\sigma cl_\alpha}{16} - \frac{V_A}{2\Omega R}\right)^2 + \frac{\sigma cl_\alpha}{8}\theta\frac{r}{R} +}$$
$$-\left(\frac{\sigma cl_\alpha}{16} - \frac{V_A}{2\Omega R}\right) \qquad (10)$$

where $\sigma$ represents the ratio between the blade aerea and the disk area. Once the converged solution of the inflow angle is derived for each blade section, the local AOA is known; integration of Equations (6) radially across the blade yields the total thrust and torque delivered by the propeller.

Thrust and torque allow the evaluation of spindle moment representing the forcing term of blade equilibrium equation about the bearing axis. For any blade section, elemental

centrifugal field is properly described by the left-hand side of Equation (2), the emphasis is here on the hydrodynamic moments induced by thrust and torque. Hence, the spindle moment forcing Equation (2) is

$$m_H^z = \int_{r_{boss}}^{R} (dM_T + dM_Q) dr \qquad (11)$$

With respect to the body-frame of reference $O, X_b, Y_b, Z_b$, $(x_p, y_p, z_p)$ define the location of the centre of pressure of the elemental section; following Miles et al (1992), these distances may be derived as a function of the blade shape. Specifically, by assuming nose-up positive pitching moments, for any hydrofoil the sectional spindle moments are

$$\begin{aligned} dM_T &= dT \, y_p \\ dM_Q &= -dF_Q \, x_p \end{aligned} \qquad (12)$$

where the local force $dF_Q = (dQ/r)cos\xi$ is shown in Figure 3, whereas

$$\begin{aligned} y_p &= r sin\xi \\ x_p &= -e_h + rtg\delta - \xi rtg\theta \end{aligned} \qquad (13)$$

with

$$\begin{aligned} d_{sp} &= d_{hd} - d_{cp} \\ \xi &= \frac{d_{sp}}{[r^2 + (r \, tg\theta)^2]^{1/2}} \end{aligned} \qquad (14)$$

The geometrical parameters appearing in Equations (13) and (14) are described in the following: $e_h$ is the blade offset fom the pivot axis, $\delta$ is the rake angle, $\xi$ is the projected angle of pressure centre with respect to $z_b$ axis whereas $d_{sp}$ defines the distance of pressure centre from the generator line. Moreover, $d_{hd}$ represents the distance of the generator line from the leading edge of the section and $d_{cp}$ identifies the location of the centres of pressure from the leading

edge. To determine $d_{cp}$, the knowledge of the pitching moment coefficient (with respect to a given point) as a function of the AOA and the Reynolds number is needed; function $cm = cm(\alpha, Re)$ may be derived from tabular data, experiments or by using a devoted hydrodynamic analysis of blade sections. Whatever the choice is, the centre of pressure position, measured from the leading edge, is given by

$$d_{cp} \cong c \, \frac{cm}{cl \, cos\alpha} \qquad (15)$$

The effects induced by the variation of $a$ and $a'$ across the blade width on the pitching moment $cm$ may be modelled through the scheme proposed by Ludwieg and Ginzel (see Miles et al 1992); specifically, the corrected pitching moment $cm_c$ is

$$cm_c = cm \, (\frac{m}{c}) + \mu(k1 \, k2 - 1)cl_i \qquad (16)$$

where $m/c$ is the camber-chord ratio, $\mu$ is a parameter depending on the mean-line shape of the hydrofoil and operating conditions, $k1$ and $k2$ are the camber correction coefficients (see Eckhardt et al 1955) whereas $cl_i$ is the ideal lift coefficient.

### 3.2 Boundary Element Method

In the present work a propeller hydrodynamics model based on a Boundary Element Method (BEM) is also considered here as an approach to overcome limitations of BEMT in providing a general representation of three-dimensional flow effects around arbitrarily shaped bodies. Starting from mass and momentum conservation equations for an incompressible flow, a general formulation to describe a three-dimensional body arbitrarily moving with respect to a fluid is derived. The methodology is applied here to the case of a marine propeller. Assuming that the incoming flow is inviscid and the velocity perturbation induced by the body is irrotational except for a thin layer of vorticity shed at propeller blades trailing edges, it is possible to introduce a scalar potential $\varphi$ and represent the perturbation velocity in gradient form as $\mathbf{v} = \nabla\varphi$. Mass conservation equation yields that the velocity potential is governed by the Laplace equation $\nabla^2\varphi = 0$, whereas the momentum equation is manipulated to obtain a direct relationship between velocity potential and flow pressure as

$$\frac{\partial\varphi}{\partial t} + \frac{1}{2}q^2 + \frac{p}{\rho} + gz_0 = \frac{1}{2}v_I^2 + \frac{p_0}{\rho} \qquad (17)$$

Equation (17), known as Bernoulli's theorem, is written in the rotating frame of reference $(O, x_b, y_b, z_b)$ introduced in Figure 1. Quantity $\mathbf{v}_I$ denotes the velocity of flow incoming to the propeller disc, $\mathbf{q} = \nabla\varphi + \mathbf{v}_I$ is the total velocity, and $gz_0$ is the hydrostatic head.

A classical derivation (see *e.g.*, Morino 1993) yields that the perturbation velocity $\varphi$ can be determined from the Laplace equation through the following elegant boundary integral representation

$$\varphi(\mathbf{x}) = \oint_{\mathcal{S}_B} \left( \frac{\partial\varphi}{\partial n}G - \varphi\frac{\partial G}{\partial n} \right) d\mathcal{S} - \int_{\mathcal{S}_W} \Delta\varphi\frac{\partial G}{\partial n}d\mathcal{S} \qquad (18)$$

where $\mathcal{S}_B$ denotes the body surface (*i.e.*, , the propeller), $\mathcal{S}_W$ is the trailing vortical surface (the wake), and $\mathbf{n}$ is the unit normal to these surfaces. The symbol $\Delta$ denotes discontinuity of $\varphi$ across the wake surface, and $G, \partial G/\partial n$ are respectively unit source and dipole singularities in the unbounded three-dimensional space. Under non-cavitating flow assumptions, Equation (18) is used to evaluate $\varphi$ and hence the velocity field on the body surface and in the fluid domain once quantity $\partial G/\partial n$ is determined by imposing the impermeability condition on $\mathcal{S}_B$ and $\Delta\varphi$ is determined by using a Kutta-type condition. The extension of Equation (18) to describe propeller cavitation is described in Salvatore et al (2003).

Once pressure on the solid surface is determined by the Bernoulli Equation (17), and denoting by $\tau$ the tangential (viscous) stress on $S_B$, hydrodynamic forces $\mathbf{f}$ and moments $\mathbf{m}_O$ acting on the propeller are computed as

$$
\begin{aligned}
\mathbf{f} &= \oint_{S_B} (-p\,\mathbf{n} + \tau\,\mathbf{t})\,dS \\
\mathbf{m}_O &= \oint_{S_B} (-p\,\mathbf{r} \times \mathbf{n} + \tau\,\mathbf{r} \times \mathbf{t})\,dS \qquad (19)
\end{aligned}
$$

where $\mathbf{r} = \mathbf{x} - \mathbf{x}_O$, $\mathbf{t}$ is the unit tangent to $S_B$ aligned to local streamlines. Propeller thrust $T$ and torque $Q$ easily follow by taking axial components of $\mathbf{f}$ and $\mathbf{m}$ respectively. Next, spindle moment $m_H^z$ is evaluated as the component of $\mathbf{m}_O$ along the blade spindle axis.

Recalling BEM is based on inviscid-flow assumptions, additional modelling is required to predict the tangential stress $\tau$ and hence to estimate viscosity contributions to propeller loads in Equation (19). The problem is analysed in Salvatore et al (2003) where a coupled BEM/bounday-layer solver formulation is described. In the present work, a semi-empirical approach is used in which local distribution of $\tau$ on blade surface is derived from classical laws for attached laminar and turbulent boundary layer on a flat plate. If local effective angle of attack is higher than a prescribed threshold, viscosity effects in Equation (19) are further corrected to approximately account for the additional drag induced by boundary layer flow separation.

The evaluation of the effective angle of attack implies that a correct prediction of the velocity distribution induced by the propeller wake is achieved. To this aim, a trailing wake alignment procedure is used in which the location of the wake surface $\mathcal{S}_W$ in Equation (18) is determined as a part of the flowfield solution. Details of this approach and numerical applications are described in Greco et al (2004).

### 3.3 Reduced-Order Hydrodynamics Model

In this section a theoretical discussion on the identification of a linear Reduced Order Model (ROM) describing the unsteady hydrodynamic forces arising on the propeller blades of a SPP when perturbed from their equilibrium pitch setting is outlined. The proposed methodology has been developed and fully validated for rotorcraft aeroelasticity applications (see Gennaretti et al 2005, 2008 and Serafini et al 2009). It is valid for rotorcraft configurations where the rotor wake develops along the axial direction.

For an isolated SPP propeller in cruise conditions in a potential non–cavitating uniform flow, the image of perturbation velocity of an arbitrary blade point $\vec{x}$, in the blade frame of reference, is given by

$$\vec{v}^d(\vec{x}, t) = \vec{\omega}(t) \times (\vec{x} - \vec{x}_O) \qquad (20)$$

As shown in Gennaretti et al (2005), the velocity distribution in Equation (20) can be expressed as $\vec{v}^d(\vec{x}, t) = \dot{q}(t) \, \vec{\Psi}(\vec{x})$ where $q(t) = \epsilon(t)$ is the generalized coordinate of blade rigid body motion and $\vec{\Psi}(\vec{x})$ is a time-independent vector spatial distribution derived from Equation (20).

Under the assumption of linear analysis, a suitable formulation for Equation (18) in the frequency-domain is obtained. Expressing blade surface boundary conditions $\frac{\partial \varphi}{\partial n}$ as functions of blade's point velocity $\vec{v}^d$, coupling the solution for the velocity potential with Bernoulli's theorem and dropping reference–state terms, perturbation hydrodynamic moment acting on each propeller blade corresponding to perturbative blade rigid motion about the spindle axis can be expressed, in the frequency domain, by the following matrix form (see, for details, Gennaretti et al 2005)

$$\tilde{\mathbf{m}} = \mathbf{E}(s) \, \tilde{\mathbf{q}} \qquad (21)$$

where $\mathbf{E}(s)$ is the $[Z \times Z]$ hydrodynamic transfer-function matrix that relates generalized coordinates of blade rigid motion, to the corresponding hydrodynamic moment acting on the blade. Note that the introduction of a BEM 3D solver capable to take into account mutual hydrodynamic interference among the blades yields that the hydrodynamic moment acting on the $n-th$ blade is influenced by the motion of all the other blades about their spindle axis. Thus in general the $Z$-element column matrix $\mathbf{q}$ collects the $Z$ generalized coordinates of blades rigid body motion $q_n(t)$. Entries of matrix $\mathbf{E}$ are transcendental function of the Laplace variable, $s$, because of the flow unsteadiness induced by the vorticity shedding process behind and below each rotor blade. Such aerodynamic operator would give rise to an infinite-dimension state space problem in the time-domain and is not convenient for direct inclusion in the dynamics equations to be applied for stability analysis purposes. Thus, in order to identify the aerodynamic ROM, rational expressions for approximating the transfer functions in the aerodynamic matrix are used. As shown in Morino et al (1995), the following approximate rational-matrix expression is derived for the hydrodynamic transfer-function matrix

$$\mathbf{E}(s) \approx s^2 \, \mathbf{A}_2 + s \, \mathbf{A}_1 + \mathbf{A}_0 + \mathbf{C} \left[ s \, \mathbf{I} - \mathbf{A} \right]^{-1} \mathbf{B}, \qquad (22)$$

where matrices $\mathbf{A}_2$, $\mathbf{A}_1$ and $\mathbf{A}_0$ have dimensions $[Z \times Z]$. In addition, $\mathbf{A}$ is a square matrix with dimensions $[N_a \times N_a]$, $\mathbf{C}$ is a $[Z \times N_a]$ matrix, and $\mathbf{B}$ has dimensions $[N_a \times Z]$. Next, combining Equation (22) with Equation (21) and transforming into time domain, the following constant-coefficient ROM relating the generalized rigid blade motion coordinates (and their time derivatives) with the corresponding unsteady hydrodynamic moments arising on the perturbed blades is obtained:

$$\mathbf{m}(t) = \mathbf{A}_2 \ddot{\mathbf{q}} + \mathbf{A}_1 \dot{\mathbf{q}} + \mathbf{A}_0 \mathbf{q} + \mathbf{C} \, \mathbf{r}$$
$$\dot{\mathbf{r}} = \mathbf{A} \, \mathbf{r} + \mathbf{B} \, \mathbf{q}, \qquad (23)$$

where $\mathbf{r}$ is the column matrix that collects the $N_a$ additional hydrodynamic states associated to the poles included in the approximating aerodynamic matrix (a consequence of the flow-memory effects included in matrix $\mathbf{E}$).

The proposed model allows time–domain evaluation of the hydrodynamic loads on propeller blades as explicit functions of the system degrees of freedom $\mathbf{q}$ and of a finite number of additional (hydrodynamic) states.

## 4 NUMERICAL APPLICATIONS

Theoretical and computational methodologies described above are here applied to study the performance of two different kind of propellers in uniform flow conditions. A preliminary analysis on conventional Controllable-Pitch Propellers is presented to assess spindle moment numerical predictions. In fact, the analysis of CPP typically includes estimations of blade spindle moments to achieve a correct sizing of pitch control mechanisms.

| Blades number, $Z$ | 5-CPP |
|---|---|
| Propeller diameter, $D$ | 234.29 mm |
| Nominal pitch, $P/D_{r07}$ | 1.061 |
| Expanded area ratio | 0.829 |
| Skew ($r/R = 0.7$) | 6.44° |
| Rake ($r/R = 0.7$) | 0.0 mm |
| Hub/Propeller diameter ratio | 0.29 |
| Blade sections airfoil | NACA 16 (mod) + NACA65 meanline |

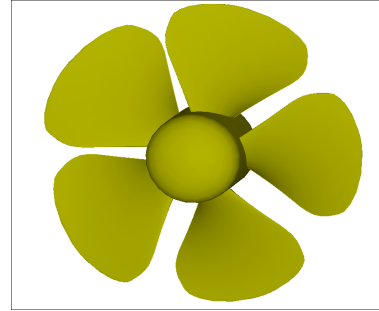Table 1: DTRC P4402 controllable-pitch propeller main geometry parameters.



Figure 4: Three-dimensional model of DTRC-P4402 Controllable-Pitch Propeller.

An extensive experimental study on CPP has been documented by David Taylor Research Center (see Boswell et al 1975). Among different propeller models tested, the DTRC P4402 model is chosen here. Main geometry parameters are shown in table 1 whereas a three-dimensional sketch of the propeller is shown in figure 4. Propeller open water characteristics are shown in Figure 5. Experimental data in Boswell et al (1975) describing propeller thrust, torque and spindle moment coefficients ($K_T$, $K_Q$ and $K_S$,
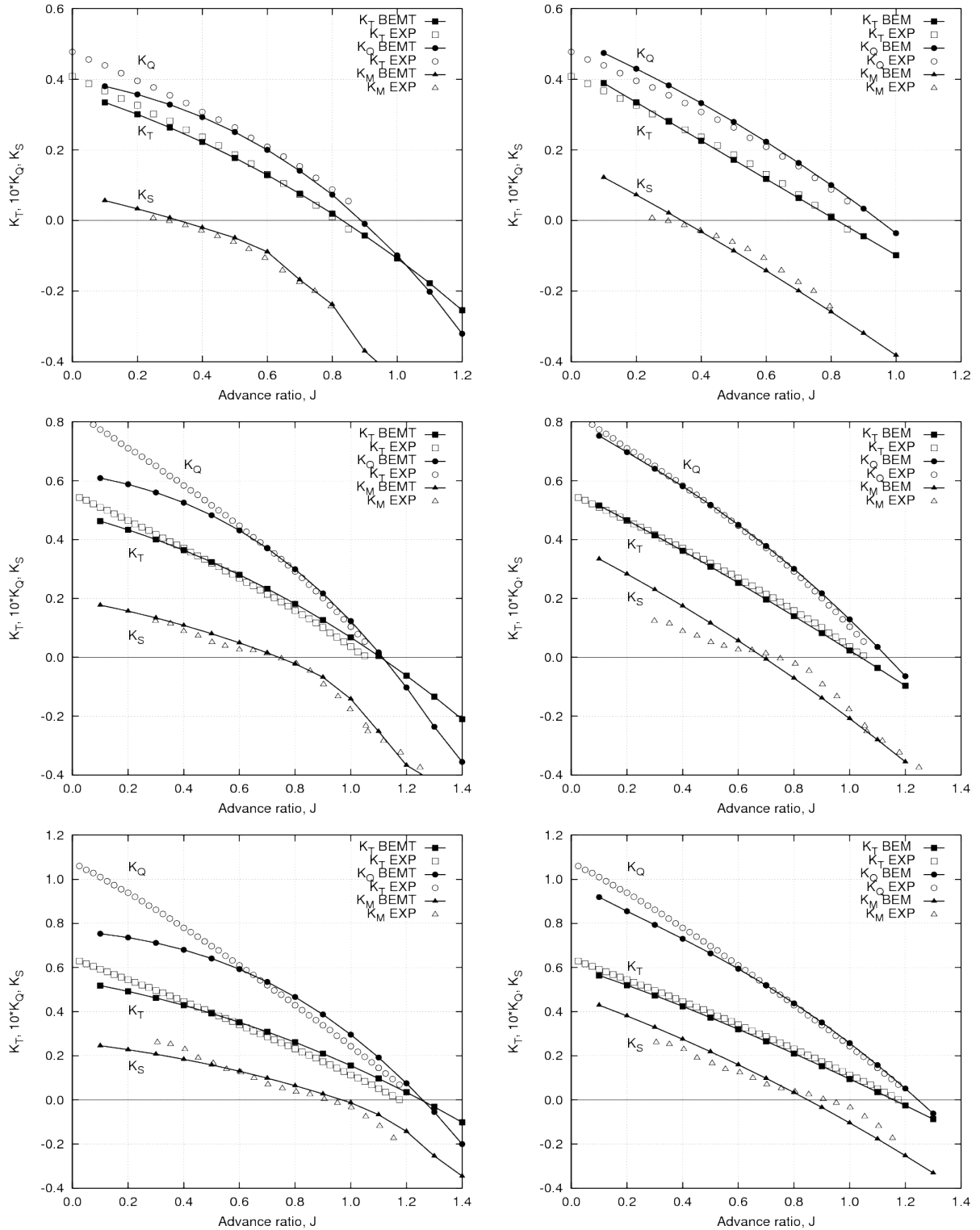
Figure 5: DTRC P4402 CPP performance ($K_T$ and $K_Q$) and spindle moment ($K_S$): numerical predictions compared to measurements at $P/D = 0.8$ (top), $P/D = 1.061$ (center) and $P/D = 1.2$ (bottom).

respectively) are compared to corresponding quantities evaluated by BEMT and BEM. Three different blade pitch settings are considered: $P/D = 0.8$, $P/D = 1.061$ (design) and $P/D = 1.20$. At $P/D = 0.8$ (see Figure 5, top) BEMT performance predictions show a general

good agreement with BEM predictions and with experimental data. For low $J$ values (minor than $0.4$), BEMT predictions tend to slightly underestimate $K_T$ and $K_Q$ whereas BEM overestimates $K_Q$. These discrepancies can be explained considering the difficulties in modelling

viscous flow phenomena in both models. Moreover, at these low $J$ values, the effect of trailing wake shed by blades is more relevant; thus further enhancements of BEMT capability to describe 3D inflow are expected to improve numerical predictions. The comparison between BEMT results and experimental ones in terms of spindle moment are excellent; this is due to a tuning process on flow-curvature correction tailored to fitting experiments. On the contrary, the agreement between BEM results and experimental data is satisfactory in terms of trend, even though some discrepancies are evident. However, this drawback in capturing pitching moments is within the accuracy of BEM approaches. Note that plotted measured spindle moment coefficient is magnified by a factor 50 whereas numerical predictions are multiplied by 20 in order to fit into the same diagram as thrust and torque coefficients. It is important to observe that BEMT and BEM predicted $K_S$ sign inversion conditions are in good agreement with results of model tests. Reliable predictions of blade spindle moment values in the inversion region are fundamental for a correct estimation of self-pitching propeller behaviour. Finally, as $J$ increases towards the zero thrust point ($J = 0.82$), an increasing part of the blade works at negative angles of attack. A careful tailoring of the flow curvature modelling in BEMT is then required. Figure 5 (center) shows that, for design pitch setting $P/D = 1.061$, $K_T$ predictions by BEMT are in good agreement with respect to BEM simulations and experimental data. Discrepancies are highlighted at very low values of $J$ due to viscosity and trailing wake induced phenomena not accurately modelled in the BEMT solver, whereas, for $J > 0.9$ the lack of hub modelling can explain the overestimated values of thrust (the presence of the hub has the effect of a local acceleration of the inflow to blade sections). Also in this case, spindle moment predictions by BEMT are excellent with respect to measurements. Specifically, $J$ value corresponding to the inversion is very well captured. Discrepancies in BEM predictions for $J < 0.6$ and $0.75 < J < 0.9$ arise from the numerical issues previously pointed out. Finally, $P/D = 1.2$ pitch setting is considered. Figure 5 (bottom) confirms the capability of the present BEMT to predict CPP performance and spindle moment over a wide range of operating conditions. The specific enhancements introduced in the BEMT model to take into account flow curvature effects on spindle moment yields that $K_S$ predictions are in very good agreement with respect to measurements even if some discrepancies at low $J$, corrisponding to thrust vanishing region, are evidenced on $K_T$ and $K_Q$. For those operating conditions modelling of viscous flow phenomena, hub presence effect, trailing wake modelling and careful evaluation of blade hydrofoils friction characteristics are crucial issues.

Since BEMT seems to be more adequate for the description of spindle moment, in the following the analysis of SPP behaviour is addressed through this approach. Next, BEMT predictions for an SPP propeller are compared to experimental data in terms of performance and prediction of equilibrium pitch setting. Among a wide set of Self-Pitching Propellers considered in Miles et al

(1992), test case no. 2 and 3 are herein addressed. Main geometry parameters are shown in table 2 whereas a sketch of a three-dimensional model of the propeller is shown in figure 6. First, three different values of fixed

| Blades number, $Z$ | 3-SPP |
|---|---|
| Propeller diameter, $D$ | 300.0 mm |
| Design nominal pitch, $P/D$ | 1.0 (const.) |
| Blade area ratio | 0.39 |
| Linear skew at tip | $-96.0$ mm |
| Rake | $8°$ |
| Hub/Propeller diameter ratio | 0.233 |
| Offset | 54.0 mm, 60.0 mm |
| Blade sections airfoil | NACA symmetric |

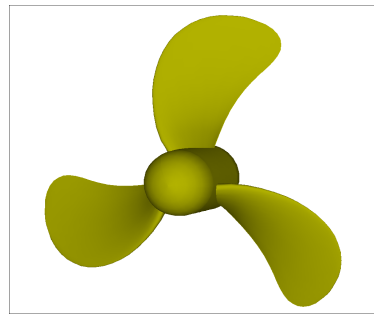Table 2: P2 self-pitching propeller main geometry parameters.



Figure 6: Three-dimensional model of P2 Self-Pitching Propeller.

pitch setting are considered: $P/D = 0.4$, $P/D = 0.8$ and $P/D = 1.2$. BEMT predictions in terms of $K_T$ and $K_Q$ are compared to measurements and to numerical results by Miles et al (1992) based on a BEMT approach similar to the one proposed here (indicated with WU in the following). From the physical standpoint, a different propeller offset affects only spindle moment. Nevertheless this is not confirmed by experimental results. In fact, there is a relevant discrepancy between $K_T$ and $K_Q$ measured on propeller no. 2 ($e_h = 54$ mm) and no. 3 ($e_h = 60$ mm). This could be explained, as suggested by the authors, by an uncertainty in the pitch/diameter ratio setting of about 0.05 around the nominal $p/D$ at 70% of blade radius. For these reasons the performed numerical analysis addresses not only nominal pitch setting for propeller no. 2 but also investigates the effect of a 0.05 change of pitch setting on performance predictions.

Figure 7 (top) shows performance curves for propeller no. 2 at nominal $p/D = 0.4$. Experimental and numerical results given by Miles et al (1992) are compared to numerical results by the present BEMT approach. At this nominal pitch condition only experimental and numerical results for propeller no. 2 are available. BEMT predictions shown in the figure are performed at $p/D = 0.35$, $0.40$, and $0.45$ to
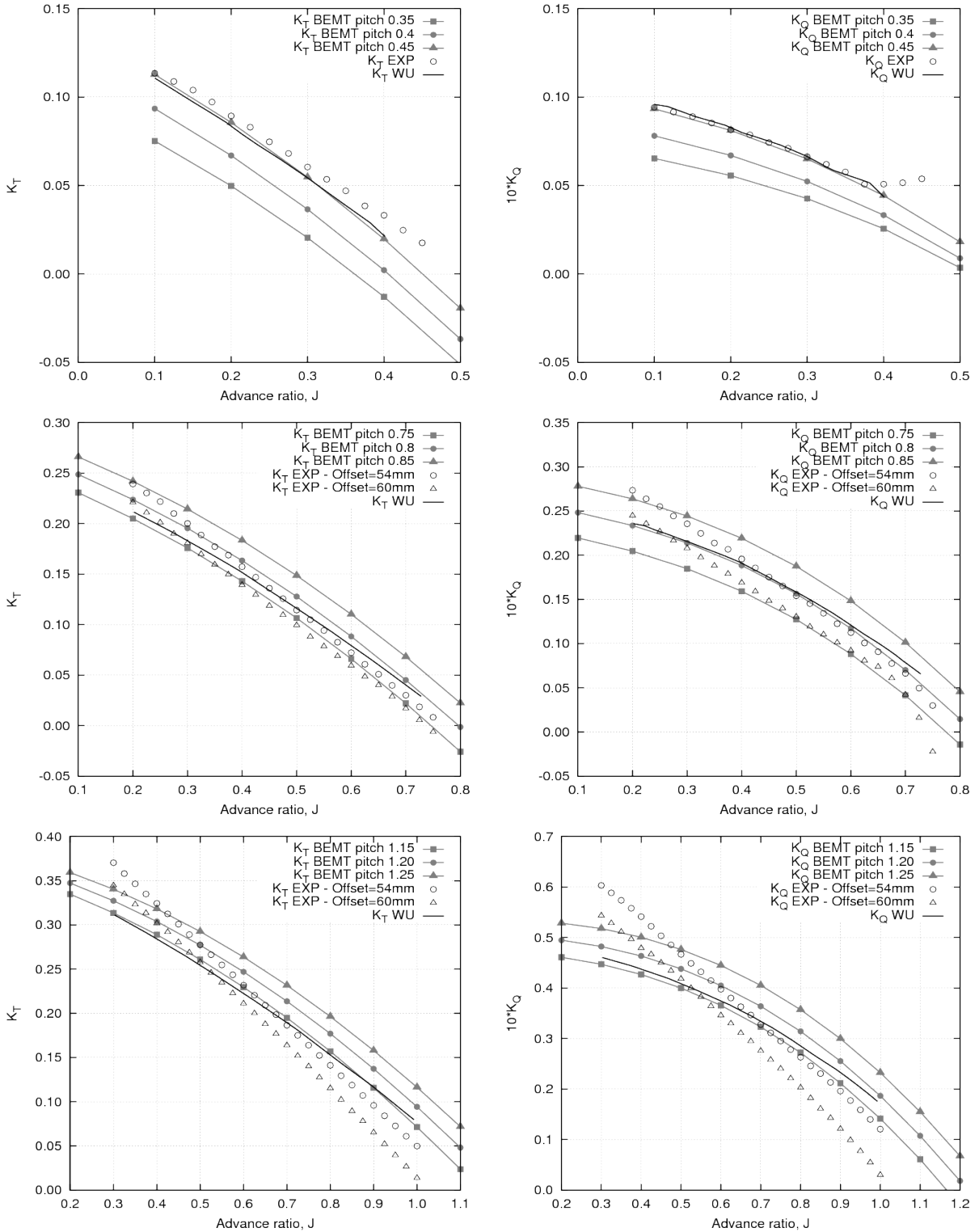
Figure 7: SPP-P2 propeller performance ($K_T$, top, and $K_Q$, bottom): numerical predictions compared to measurements at $P/D = 0.35, 0.40, 0.45$ (top), $P/D = 0.75, 0.80, 0.85$ (center) and $P/D = 1.15, 1.20, 1.25$ (bottom).

investigate the effect of pitch uncertainty on loads predictions. Both for $K_T$ and $K_Q$ the agreement between BEMT predictions, measurements and numerical WU-BEMT data is very good if $p/D = 0.45$ is considered in the simulations. It should be noted that experimental $K_Q$ curve

shows a very unusual trend for $J > 0.4$. Next, $p/D = 0.8$ pitch setting is considered. In this case experimental data are available for both propeller no. 2 and 3 and Figure 7 (center) clearly evidences discrepancies of $K_T$ and $K_Q$ measured data for these two propellers. For this configu-

ration $K_T$ BEMT numerical predictions for $p/D = 0.75$ and $p/D = 0.80$ fall within experimental uncertainty and are comparable to WU-BEMT predictions. At nominal $p/D = 0.8$ setting BEMT predictions tend to slightly overestimate measured propeller thrust whereas torque is very well catpured if $p/D = 0.75$ and $p/D = 0.80$ BEMT simulations are considered. Finally, for $p/D = 1.2$, Figure 7 (bottom) shows the same comparison as above. In this case, numerical $K_T$ predictions by the present BEMT model for $p/D = 1.15$ are in good agreement with WU-BEMT results. Moreover, if $p/D = 1.15$ is considered, BEMT predictions tend to slightly overestimate thrust for $J > 0.8$. This effect can be explained by considering the peculiar geometry of SPP hubs that has a major impact on propeller performance predictions at high values of $J$. Thrust underestimation due to viscosity and wake effects at $J < 0.5$ are evidenced. Torque predictions by BEMT are also in good agreement with experimental and WU-BEMT numerical results for propeller no. 2 whereas, viscosity and wake induced effects on torque yield discrepancies for $J < 0.6$.

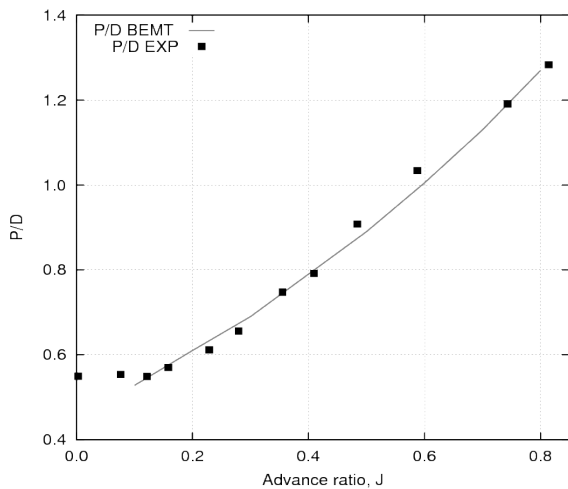Finally, the equilibrium pitch setting for propeller no.



Figure 8: Numerical predictions of P2 free pitching equilibrium conditions compared to measured data.

2 is addressed. Figure 8 shows BEMT numerical predictions compared to measured data from Miles et al (1992). In the operating range herein considered, BEMT hydrodynamics solver shows a very good capability to capture experimental equilibrium conditions. It is worth noting that the considered operating range is limited to $J$ values yielding equilibrium pitch settings where numerical predictions by BEMT are reliable based on experience gained from the previous fixed pitch analysis. At $J$ values higher than 0.8 (and pitch settings greater than $p/D = 1.2$) further assessment of BEMT capability to accurately describe SPP hydrodynamics is deemed necessary.

### CONCLUSIONS

The development and assessment of computational methodologies for the analysis and design of Self-Pitching Propellers (SPP) has been presented to determine blade free-pitching conditions. Two complementary hydrodynamics approaches based on Blade Element Momentum Theory (BEMT) and Boundary Element Method (BEM) formulations, respectively, have been used to provide the forcing terms in the blade motion equation. Moreover, in order to address blade stability margins predictions, a Reduced Order Model based on BEM for blade unsteady loads to be coupled to the equation describing blade perturbative motion about the spindle axis has been treated from a theoretical point of view.

Numerical predictions by BEMT have been compared to available experimental results and to numerical results by BEM. An analysis on conventional Controllable-Pitch and Self-Pitching Propellers has been presented to assess both performance and spindle moment numerical predictions. Numerical results show that the simplified BEMT model is well suited to capture propeller performance as well as spindle moment and blade equilibrium condition once a devoted tailoring process is performed on the flow-curvature correction effects. In particular, numerical results demonstrate that careful tuning of model parameters can provide excellent agreement between measured and predicted spindle moment values. A similar approach can be applied to improve thrust and torque predictions. Nevertheless, more consistent estimates of the induced velocity due to the shed wake should improve capturing physical effects and should reduce the impact on results of empirical corrections applied *e.g.*, , to adjust the blade pitching moment. Present computational studies also highlight that corrections to better describe viscosity-induced features like cross flow on the blade surface and boundary layer separation are also important but they do not affect the overall quality of numerical results as flow-curvature correction does.

A fully three-dimensional hydrodynamics model by BEM has shown to be adequate to analyse major aspects affecting CPP performance over a wide range of operating conditions. The appeal of such a computational approach is that a consistent description of three-dimensional, unsteady flow around an arbitrarily shaped body is provided whilst semi-empirical corrections are relevant only in those cases where viscous-flow separation occours on large portions of the blade surface. Calculated propeller thrust and torque are typically reliable, whereas some numerical issues may arise in the prediction of blade spindle moment.

In summary, the proposed theoretical and computational methodology represents a sound basis for the analysis of SPP performance, for the prediction of self-pitching conditions and of the corresponding stability analysis of blade equilibrium about the spindle axis.

Further research will be focused on the improvement of BEM spindle moment predictions and the inclusion in BEMT of the induced velocity calculated by the three-dimensional hydrodynamics solver taking into account trailing wake effects. Applications of the proposed ROM to SPP stability margins will be also investigated.

## REFERENCES

Boswell, R.J., Nelka, J.J., Kader, R.D. (1975). 'Experimental Spindle Torque and Open-Water Performance of Two Skewd Controllable-Pitch Propellers'. David W. Taylor Naval Ship Research and Development Center Technical Report, **4753**, Bethesda (MA), USA.

Carlton, J.S. (ed.) (1994). Marine Propellers and Propulsion. Oxford: Butterworth & Heinemann Ltd.

Eckhardt, M.K. & Morgan, W.B. (1955). 'A Propeller Design Method'. Transactions of the Society of Naval Architects and Marine Engineers in Marine Engineers in America (SNAME), **63**, pp. 325–374.

Gennaretti, M. & Greco, L. (2005). 'A Time–Dependent Coefficient Reduced–Order Model for Unsteady Aerodynamics of Proprotors'. Journal of Aircraft, **42**(1), pp. 138–147.

Gennaretti, M. & Greco, L. (2008). 'Whirl flutter analysis of prop–rotors using unsteady aerodynamics reduced–order models'. The Aeronautical Journal, **112**(1131), pp. 233–242.

Greco, L., Salvatore, F., & Di Felice, F. (2004). 'Validation of a Quasi–potential Flow Model for the Analysis of Marine Propellers Wake'. Twenty-fifth ONR Symposium on Naval Hydrodynamics, St. John's, Newfoundland (Canada).

Leishman, J. G. (ed.) (2006). Principles of Helicopter Aerodynamics. Cambridge University Press 2006, second edition.

Miles, A., Wellicome J.F., & Molland, A.F. (1992). 'The Technical and Commercial Development of Self-Pitching Propellers'. Meeting of the RINA - The Royal Institution of Naval Architects, Southampton, UK.

Morino, L. (1993). 'Boundary Integral Equations in Aerodynamics'. Applied Mechanics Reviews **46**(8), pp. 445–466.

Morino, L., Mastroddi, F., De Troia, R., Ghiringhelli, G.L. & Mantegazza, P. (1995). 'Matrix fraction approach for finite-state aerodynamic modeling'. AIAA Journal **33**(4), pp. 703–711.

Salvatore, F., Testa, C., & Greco, L. (2003). 'A Viscous/Inviscid Coupled Formulation for Unsteady Sheet Cavitation Modelling of Marine Propellers'. Proceedings of CAV 2003 Symposium, Osaka, Japan.

Serafini, J., Greco, L. & Gennaretti, M. (2009). 'Prediction of rotorcraft-pilot coupling phenomena through reduced-order aerodynamic model'. Proceedings of the International Forum on Aeroelasticity and Structural Dynamics - IFASD2009, Seattle (WA), USA.